







TECHNICAL ARTICLE

# Manufacturing Processes for Permanent Magnets: Part II—Bonding and Emerging Methods

JUN CUI<sup>1,2,3,7</sup>  JOHN ORMEROD<sup>1,4</sup> DAVID S. PARKER<sup>1,5</sup>  
RYAN OTT<sup>1,2</sup>  ANDRIY PALASYUK<sup>1,2</sup> SCOTT MCCALL<sup>1,6</sup>  
MARIAPPAN PARANS PARANTHAMAN<sup>1,5</sup>  MICHAEL S. KESLER<sup>1,5</sup>  
MICHAEL A. MCGUIRE<sup>1,5</sup> CAJETAN NLEBEDIM<sup>1,2</sup>   
CHAOCHAO PAN<sup>1,2,3</sup> and THOMAS LOGRASSO<sup>1,2,3</sup>

1.—Critical Materials Institute, Ames, IA 50011, USA. 2.—Ames Laboratory, Ames, IA 50011, USA. 3.—Material Science and Engineering Department, Iowa State University, Ames, IA 50011, USA. 4.—JOC LLC, Loudon, TN 37774, USA. 5.—Oak Ridge National Laboratory, Oak Ridge, TN 37831, USA. 6.—Lawrence Livermore National Laboratory, Livermore, CA 94550, USA. 7.—e-mail: cuijun@ameslab.gov

Permanent magnets produce magnetic fields and maintain the field even in the presence of an opposing magnetic field. They are widely used in electric machines, electronics, and medical devices. Part I reviews the conventional manufacturing processes for commercial magnets, including Nd-Fe-B, Sm-Co, alnico, and ferrite in cast and sintered forms. In Part II, bonding, emerging advanced manufacturing processes, as well as magnet recycling methods are briefly reviewed for their current status, challenges, and future directions.

## INTRODUCTION

A permanent magnet can produce and maintain a magnetic field even in the presence of an opposing magnetic field. In comparison, an electromagnet does not produce a magnetic field on its own. It relies on electric currents to generate the magnetic field. Obviously, energy conversion systems powered by permanent magnets will use less energy than those using electromagnet. Currently, all the best performing magnets for electrical machines contain rare earth (RE) elements. Nd-Fe-B is the most potent magnet at room temperature, with maximum energy product  $(BH)_{\max}$  exceeding 55 MGOe for commercial products.<sup>1–4</sup> Other magnets without RE materials are much less powerful: 10 MGOe for Alnico<sup>5</sup> and only 5 MGOe for ferrite magnets.<sup>6</sup> Consequently, the Nd-Fe-B magnet is the most popular choice for a wide range of applications, from home appliances to military devices and electric vehicles to wind turbines. Nd and Dy are critical materials due to the growing demand and constrained supply.

Intensive efforts are ongoing to mitigate the RE elements' criticality, including increasing supply, reducing waste, and developing alternatives. For example, instead of using Dy to sustain a PM's coercivity at high temperatures, smaller grain sizes could achieve the same effect. However, such an engineering approach requires a demanding manufacturing process to realize its potential. Other efforts focus on how to reduce production waste and improve the consistency of a PM's performance. Improving the manufacturing process appears to be a viable near-term approach to mitigate the RE criticality issue.

There are several common and less common manufacturing processes for making permanent magnets. In Part-I of the review article, the common manufacturing processes for cast and sintered PM including Nd-Fe-B, Sm-Co, Alnico, ferrite were reviewed. In Part-II, manufacturing processes for the bonded magnets and less common or emerging magnet manufacturing processes such as extrusion, additive manufacturing, spark plasma sintering, shock compaction, and thermomagnetic processing are reviewed for their current status, challenges, potentials, and future directions.

## COMMON MAGNET FABRICATION PROCESSES: BONDING

Bonded magnets are an important but often overlooked group of products that magnetic circuit and device designers should consider when choosing the optimum permanent magnet type for their specific application needs.<sup>7</sup> In their most basic form bonded magnets consist of two components: a hard-magnetic powder and a non-magnetic polymer or rubber binder. The powder may be hard ferrite, Nd-Fe-B, Sm-Co, Sm-Fe-N, or mixtures of magnetic powders known as hybrids. The binder that holds the magnetic particles in place can produce either a flexible or rigid matrix. Typical binders for flexible magnets are nitrile rubber and vinyl. Binders for rigid magnets include nylon, PPS, polyester, Teflon, and thermoset epoxies. The thermoplastic binders may be formed into sheet via calendering or extrusion or formed into various complex shapes using injection molding. Compression bonding almost exclusively combines isotropic Nd-Fe-B powders with a thermoset epoxy binder using a uniaxial room temperature pressing process. A major advantage of bonded magnet processing is that near net shape manufacturing requires zero or minimal finishing operations compared to powder or cast metallurgical processes. In addition, value added assemblies can be economically produced in a single operation.

General Motors (spun off as Magnequench in 1986) pioneered the use of melt spinning to produce isotropic Nd-Fe-B powders which are used primarily in bonded magnet production, either compression bonding or injection molding. The principle of melt-spinning consists of melting the alloy or elements in a crucible under vacuum or inert gas. The melt, under inert gas pressure, is sprayed through an orifice in the crucible onto a rotating, water-cooled copper wheel or disc. Cooling rates  $> 1,000,000$  °C/sec can be achieved which produces an alloy with an amorphous or fine grained nanocrystalline structure.

There are four main processing routes used to manufacture most bonded magnets: calendering, injection molding, extrusion, and compression bonding. Figure 1 shows their typical processing schematics, feedstock, products, and equipment.

Calendering is a rolling process for making continuous magnet sheets. It is used for flexible, rubber-based magnets and most often uses ferrite powders, though some Nd-Fe-B and ferrite/Nd-Fe-B hybrids are available. The granulated compound of magnetic powder and elastomer is fed from the top and through a series of heated rolls. High compressive load is applied by the roller to the feedstock powders and tension is applied to the sheet as it exits the rollers. A continuous roll of several hundred feet can be formed. In some cases, texture can be achieved due to the applied pressure and utilizing the plate-like shape of the ferrite particles.

Injection molding is the process of injecting a molten, highly filled thermoplastic compound into mold cavities where it can cool and solidify. Ferrite and Nd-Fe-B powders are commonly used as the magnetic powder in the compound. Typically, multicavity tooling is used to achieve high volume output and productivity. Complex shaped magnets can be formed by this process together with multicomponent assemblies by insert molding and over molding techniques. Standard magnetic powder loadings are around 65 vol.%.

Extrusion process uses raw materials similar to the compound used in calendering. The extrusion screw works against a heated barrel to push the compound through a heated die at high pressure. The resulting continuous strip of material is collected, by either stacking the sheet on a spool, or cutting it into pieces of specific length. The cross-section profile of the strip remains the same along the length of the extrusion. It should be noted that since both ferrites and Nd-Fe-B powders are very abrasive, special wear resistant coatings are used in both injection molding and extrusion tooling.

Compression bonding process starts with Nd-Fe-B powder refinement and liquid encapsulating processes to coat each particle with a thin film of thermoset epoxy and hardener and other additives e.g. die wall lubricant. The encapsulated powder is fed into a press cavity and compacted under pressures of about 6 tons/cm<sup>2</sup>. The compacted magnet is then cured at temperatures of about 150–175°C. One major advantage of compression bonding is that the magnetic loading can exceed 85% by volume, resulting in higher flux densities than calendered, injection molded, and extruded magnets. Dimensional tolerances are equivalent to injection molded products, making secondary operations generally unnecessary. The development of compression bonded Nd-Fe-B with maximum energy products of 10 MGOe and higher along with net shape capability of arcs and cylinder shapes have found applications in brushless DC (BLDC) motors and Halbach array magnets.<sup>8,9</sup>

A major advantage of isotropic Nd-Fe-B magnetic powders is that no aligning field is required during forming process, simplifying the fabrication process. And since there is no residual magnetization to attract ferromagnetic particles to the magnets, it is clean during subsequent handling and assembly operations. Consequently, anisotropic Nd-Fe-B and Sm-Fe-N powders have only had a minor impact on bonded magnet applications. One significant drawback of both types of powders encapsulated with epoxy is their thermal stability and relatively low maximum operating temperature capabilities 175°C.<sup>10</sup>

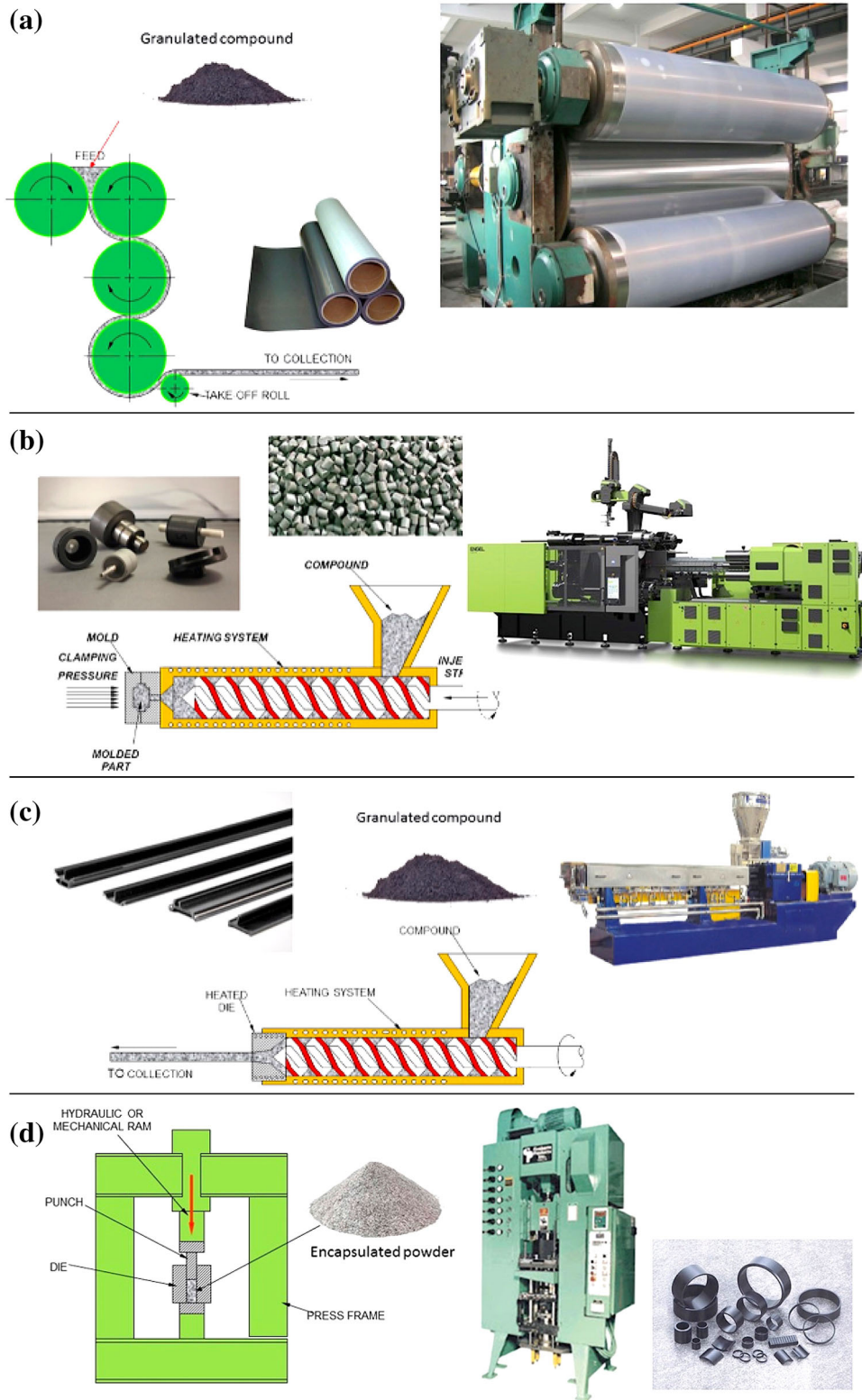


Fig. 1. Processing schematics, feedstock, products, and equipment for (a) Calendaring process for making bonded magnet sheet. (b) Injection molding bonded magnet, (c) extrusion of bonded magnet, (d) compression of bonded magnet.



## LESS COMMON AND NOVEL MAGNET FABRICATION PROCESSES

### Additive Manufacturing

Additive manufacturing (AM) is a rapidly growing area that enables production of complex, near net-shape parts with minimal loss of material. These approaches found early adoption with high-cost materials such as producing complex titanium structural parts for the aerospace industry and are particularly attractive for rare-earth permanent magnets. The ability to produce complex shapes enhances the design flexibility where machining costs of brittle permanent magnet materials often makes them cost-prohibitive. A number of advanced motor topologies promise better control of magnetic flux paths if magnets with sufficient performance can be produced.<sup>11</sup>

#### *3D Printing of Bonded Magnet via Binder-Jet and Extrusion*

Layer-by-layer three-dimensional (3D) printing enables near-net shape fabrication of magnets with complex shapes without any mold or tooling as required by the traditional molding methods. Additionally, it offers the ability to design functional grading into the magnet construction, where the type and quantity of magnetic powder can be varied as a function of position within the net-shaped magnet. Moreover, 3D-printed bonded Nd-Fe-B magnets exhibited better thermal stability, mechanical properties and superior magnetic properties compared to traditional injection molded magnets.

The binder-jet process uses a powder bed to build the magnet, a roller to transfer the powder from the feed tank, an inkjet print-head to spray the binder solution for binding the powders, and a powder feed to supply the powders. The printing process starts by spreading a thin layer of powders over the build area with the roller. The layer thickness is mostly determined by the powder size, typically  $\sim 70 \mu\text{m}$ . The print-head passes over the build area and selectively sprays binder onto the current layer. Once wetted, the print bed then moves to the curing area, usually heated by a heat lamp or UV source. After curing, the powder bed moves back to the original position and starts building the next layer. The process continues until all layers of the magnet part are printed. The printed isotropic magnet is placed in an oven at  $100\text{--}150^\circ\text{C}$  to cure the polymer binder.<sup>12</sup> Detailed descriptions of the process can be found in the work by Li and Paranthaman.<sup>12–15</sup>

Density is a critical factor for achieving higher magnetization. Densification of the binder-jet printed parts can be achieved by bronze infiltration during the post sintering at  $1100^\circ\text{C}$  or higher in an inert atmosphere or under vacuum. However, the high temperature of the bronze infiltration usually causes the binder-jet magnets to degrade. This problem can be addressed by infiltrating low-

melting point eutectic alloys such as  $\text{Nd}_3\text{Cu}_{0.25}\text{Co}_{0.75}$  (Nd-Cu-Co) and  $\text{Pr}_3\text{Cu}_{0.25}\text{Co}_{0.75}$  (Pr-Cu-Co) at much lower temperature  $510\text{--}550^\circ\text{C}$ . The density can be further improved to  $4.3 \text{ g/cm}^3$  (56% dense).<sup>15</sup> The intrinsic coercivity  $H_{ci}$  can be enhanced from 9.2 kOe to 16.9 kOe and 15.5 kOe after the diffusion of Nd-Cu-Co and Pr-Cu-Co, respectively.

Big area additive manufacturing (BAAM) is a system developed by Cincinnati Inc. to fabricate large parts via a material extrusion method which has produced bonded Nd-Fe-B magnets with attractive properties.<sup>16–22</sup> BAAM deposits layers of molten thermoplastics with magnet particles by extruding the material through a nozzle. The thermoplastic solidifies rapidly after deposition, allowing a large magnet to be built quickly. BAAM is flexible in particle size or shape. It can achieve higher powder loading in the thermoplastic polymers such as nylon (nylon-6,6 or -12, melting-point of  $178\text{--}180^\circ\text{C}$ ) and polyphenylene sulfide (PPS, melting point of  $275\text{--}280^\circ\text{C}$ ) compared to the traditional injection molding process.  $(BH)_{\text{max}}$  of AM bonded Nd-Fe-B magnets is proportional to the square of the magnetic powder volume fraction.<sup>21</sup> AM-nylon and AM-PPS Nd-Fe-B bonded magnets can be loaded up to 70 vol.% and 63 vol.% of magnetic particles, respectively.<sup>10,17</sup> The polymer coating on the magnetic particles protects magnet from corrosion and increases electrical resistivity and reduced eddy current loss. Figure 2 shows the schematic of the BAAM process for fabricating bonded Nd-Fe-B magnets. Magnequench isotropic MQP B+ powders or anisotropic MQA 38-14 Nd-Fe-B powders were mixed with nylon or PPS polymer binders. The thickness of the printed layers depends on the printing nozzle size (5.1 mm diameter), scanning speed (2.5 mm/s), and particle size ( $\sim 70 \mu\text{m}$ ).<sup>16,17</sup> The recent work on  $\geq 70$  vol.% loading of anisotropic Nd-Fe-B powder has led to a magnet with  $(BH)_{\text{max}}$  over 19 MGOe.<sup>21</sup>

#### *Directed Energy Deposition*

Many commercial techniques for advanced manufacturing of metals involve directed energy focused onto powder beds, where the powder is melted to create fully dense structural parts. Recently, these approaches have been applied to rare earth magnets. Early efforts were able to produce high magnetizations and the crystal structure was retained, but the microstructure that results in high coercivity was lost.<sup>23</sup> More recently, several groups have had some success using selective laser melting<sup>24</sup> and laser powder bed fusion (LPBF).<sup>25</sup> Successful approaches have all employed the Nd-Fe-B based MQP-S-11-9 powder by Magnequench, which is a highly spherical powder produced by gas atomization. The powder was initially designed to have high flowability for manufacturing of bonded magnets and is the only Nd-Fe-B

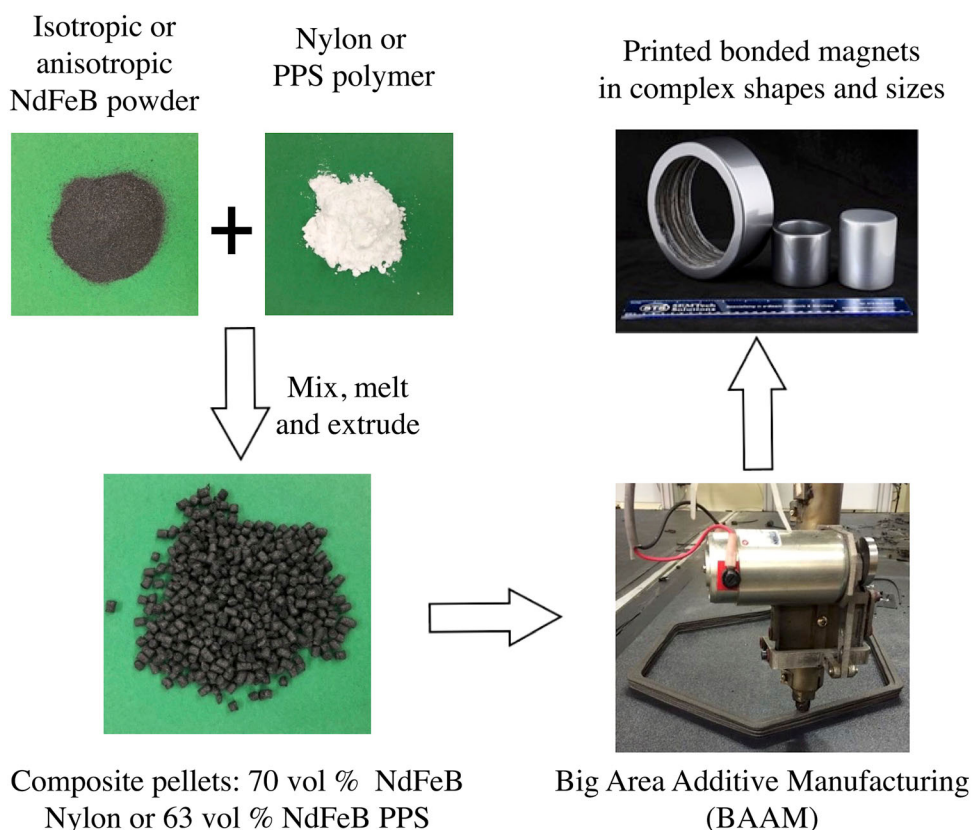


Fig. 2. Schematic of big area additive manufacturing (BAAM) process. Composite pellets are extruded into Nd-Fe-B bonded magnets with complex shapes and sizes. Printed magnets are polished and painted to achieve the smooth texture on the surface. Reprinted from<sup>10</sup> under Creative Commons License CC BY.

composition that has shown success in laser additive approaches to date, likely due to the complex composition: Nd-Pr-Fe-Co-Ti-Zr-B where Ti and Zr are known for their glass forming ability and likely helps the AM processing to retain coercivity by speeding up the laser-melt pool solidification process. The material is magnetically isotropic with a remanence of  $\sim 7.5$  kG and a coercivity of 8.4–9.4 kOe.

The first successful demonstration of 3D magnets produced by selective laser melting yielded a highly dense magnet (92%), with  $B_r$  6.2 kG,  $H_c$  8.8 kOe and  $(BH)_{\max}$  5.6 MGOe, about half that of the starting powder.<sup>26</sup> Obtaining these results required a high sweep rate for the laser with a shallow melt pool resulting in high cooling rates comparable to melt spinning ( $\sim 10^6$  °C/s), while slower sweep rates led to significantly poorer magnetic performance. Success also required printing under an inert Ar atmosphere ( $< 500$  ppm oxygen), where even at this reduced oxygen level, oxide formation from Nd was observed on the samples that had slower cooling rates. One great advantage of this approach is the design of 3D structures with complex features on the sub-millimeter scale that are not possible with traditional sintering approaches.

Directed energy approaches employing a LENS (laser engineered net shaping) system on alnico

magnets has been successfully demonstrated after appropriate heat treatments.<sup>27</sup> The desirable properties of these magnets arise from a spinodal decomposition into a nanocomposite of Fe-Co rich and Al-Ni rich particles where most of the coercivity arises from the shape anisotropy of the nanoparticles. To achieve maximum magnetic characteristics, all compositions go through a process of solutionizing, quenching, a magnetic anneal and finally a lower temperature draw.<sup>28</sup> For the LENS produced samples subjected to the standard heat treatment, the resulting magnets had magnetic properties equivalent or better than those produced by traditional sintering approaches.

### Cold Spray

Developed in the 1980s, cold spray is a material deposition process where high pressure gases are used to accelerate powder feedstock to high velocities, typically supersonic. While the gases, along with the entrained particles, are often heated to several hundred degrees Celsius, this is considered a cold process because the particles remain below their melting point. This process has primarily been used to deposit ductile powders such as aluminum and copper for repair of damaged parts, and more

recently as an additive manufacturing approach.<sup>29</sup> Most of these approaches use particles with diameters of 10–100  $\mu\text{m}$ . While the process is straightforward, only a small fraction of the sprayed material typically deposits in the area of interest, with much of the powder resulting in overspray. In many cases, this material can be recovered and reused.

More recently, cold spray including brittle materials, such as the thermoelectric  $\text{Bi}_2\text{Te}_3$ ,<sup>30</sup> has been demonstrated with smaller particles, generally 10  $\mu\text{m}$  in diameter or less, and it is a promising approach for permanent magnets where retaining the microstructure offers a wider space of materials to deposit. One route to creating cold sprayed permanent magnets has been to blend brittle Nd-Fe-B with 10–25 wt.% Al powder to serve as a binder.<sup>31</sup> This process employed commercial MQFP-B powder (Magnequench) and has been proven successful for creating fully dense coatings up to 5 mm thick on curved surfaces including on both the inside and outside surfaces of cylinders. Given that Al has a density slightly over one third that of the magnet material, even at 10 wt.% Al, the highest volume fraction of Nd-Fe-B reported to date is 68%,<sup>32</sup> resulting in a magnetic remanence of 4.9 kG. The starting powder had a remanence of 8.8 kG, so at 68% loading fraction, ideally the remanence would be about 20% higher than measured, however almost all of the coercivity is retained, with reported losses under 10% compared to the starting powder. The real advantage of this approach is the remarkable improvement in mechanical properties with ultimate tensile strengths of over 200 MPa, roughly three times larger than the sintered Nd-Fe-B magnets. Furthermore, the cold spray process creates excellent adhesion to the substrate, reducing the risk of the magnet debonding due to adhesive failure. The good mechanical properties coupled to the ability to design net shape parts make this a promising area for motor design.

## Extrusion

Decreasing grain size is effective in increasing the coercivity of permanent magnets<sup>33</sup> and a variety of approaches employing severe plastic deformation has shown success. However, for the sintered magnets, there is a lower limit to the grain size due to the size and quality of available feedstock powders. For the sintered Nd-Fe-B magnets, the coercivity does not increase further but decreases when the grain size is reduced to below 2–3  $\mu\text{m}$ . Such behavior is attributed to the increasing oxidation associated with the increasing surface area of the smaller particles. A tighter oxidation control of the manufacturing process should resolve this issue. But additional costs of equipment and labor, as well as safety concerns on handling flammable powder make the fine-grain strategy economically challenging for sintered magnet.<sup>34</sup> Hot deformation of nano-

grained coarse powders can be used to fabricate bulk magnets with sub-micron grain size, albeit the squareness of the MH loop is less than that of the sintered magnet due to the less-than-ideal texture formation. The reported hot-deformation based processes for making bulk magnet include die-upset, backward extrusion, equal channel angular extrusion, torsional extrusion, and friction consolidation and extrusion.

### *Die Upset and Backward Extrusion*

Hot-press is the most straightforward method for producing high-energy product net-shaped Nd-Fe-B magnets.<sup>35–37</sup> The process starts with rapid solidifying melt to flakes with nano-grains, ball-milling the flakes to coarse powders, then hot-pressing the powders to full density with minimal grain growth. This densification is possible in the temperature range 700–750°C because a liquid grain-boundary phase is present above 670°C.<sup>38</sup> At this stage, the magnet is still isotropic. A subsequent hot deformation produces grain alignment along the c-axis by plastic flowing at 700–800°C. Die-upsetting of the hot-pressed precursors results in anisotropic magnets with magnetization (c-axis) parallel to the press direction.<sup>39</sup> Wang et al. demonstrated a die-upset Nd-Fe-B magnet with  $(\text{BH})_{\text{max}}$  of 53 MGOe. He showed a dual-step heat treatment can improve the texture and  $B_r$  of the die-upset magnets.<sup>40</sup> Another example is the production of radially oriented ring magnets by backward extrusion.<sup>41–44</sup> The drawbacks are the additional cost of the two-steps process and limited part size/shape.

### *Equal Channel Angular Extrusion*

The equal channel angular extrusion (ECAE) process was invented in the Soviet Union roughly four decades ago,<sup>45</sup> but remained relatively unknown worldwide until the mid-1990s.<sup>46</sup> It has been mostly studied as a method for grain refinement and texture development in metallic billets.<sup>47,48</sup> It has also been used as a cold or warm compaction route for metallic, ceramic, and glassy powders.<sup>49,50</sup> ECAE is effective in imparting large shear strains in materials. The shear strain is mostly decided by the turn angle  $\varphi$ . Backpressure is another important parameter when processing powders. Bulk nanocrystalline MnAl magnet was produced from gas atomized powders using ECAE.<sup>51</sup> While over 95% green density was achieved, the texture formation was less than ideal, and the  $(\text{BH})_{\text{max}}$  was estimated at about 1 MGOe, far less than the 7 MGOe achieved with the conventional method.<sup>52</sup> Onal et al.<sup>53</sup> studied the effects of ECAP process variables on the magnetic properties of commercial meltspun Nd-Fe-Ga-Co-B powder (MQU-F1). The goal was to achieve high texture without significant grain growth. They found that higher process temperature and multiple-pass results in stronger texture formation. However,



they only obtained a 20 MGOe bulk magnet using the nanocrystalline feedstock powder with 14 kG saturation magnetization.

### *Torsion Extrusion*

Torsion extrusion, characterized by the rotation of a die during hot extrusion, has been theoretically<sup>54</sup> and experimentally<sup>55</sup> investigated for manufacturing aluminum, magnesium, copper alloys.<sup>56</sup> The process may reduce extrusion load and accumulate severe plastic deformation. Mizunuma showed that the accumulation of plastic strain by torsion extrusion is an efficient method to induce texture and refine grains of a Mg alloy.<sup>57</sup> The ability of simultaneous grain-refinement and texture-formation makes torsional extrusion an attractive method for making permanent magnets. Straumal showed that after high pressure torsion treatment the as-cast  $\text{Nd}_2\text{Fe}_{11}\text{B}$  alloy exhibits a microstructure containing nanograin  $\text{Nd}_2\text{Fe}_{14}\text{B}$  phase embedded in an amorphous matrix.<sup>58</sup> Moreover, the possibility of using coarse multi-grain feedstock powders instead of the nanocrystalline grain required by the current die-upsetting and backward extrusion methods makes torsion extrusion approach a potential transformative technology for making high performance magnets.

### *Friction Consolidation and Extrusion*

Friction consolidation and extrusion (FC&E) is a thermo-mechanical process that can be used to form fully consolidated wire, rods, tubes, or other non-circular metal shapes directly from metal precursors including powder, flake, or solid billet (Fig. 3).<sup>59</sup> It was intended as a method for making homogeneous microstructures and uniform particle distributions in fine grain metal matrix composite materials.<sup>60</sup> The FC&E process is different from the torsion extrusion process in that (1) it does not require external heating, it uses friction to generate heat; (2) the plastic deformation with the FC&E process (100–500 RPM) is much more severe than the torsion extrusion (< 10 RPM). FC&E method was explored for making bulk, highly dense, nanocrystalline Nd-Fe-B based magnets. The friction consolidation creates a layer of fully dense materials and the subsequent extrusion of this fully dense layer create an extrudate with texture depending on the material composition and die design. It can be radial or axial. A bulk Nd-Fe-B nanocrystalline magnets fabricated by FC&E exhibited  $B_r$  12.1 kG,  $H_{ci}$  11.4 kOe, and  $(BH)_{\max}$  29.8 MGOe. The nanocomposite Nd-Fe-B/Fe magnets fabricated by friction consolidation show a uniform distribution of the phases, but further process optimization is needed to reach the desired magnetic performance.<sup>59,61</sup>

## **Spark Plasma Sintering**

Spark plasma sintering (SPS), also known as pulsed electric current sintering (PECS) or field assisted sintering technique (FAST) is a sintering technique utilizing both uniaxial compressive stress and pulsed DC or AC current to consolidate powders. Joule heating plays a critical role in this unique densification process.<sup>62</sup> The internal Joule heating facilitates a very high heating and cooling rates, enhancing densification without promoting grain growth, making it possible to maintain feedstock's nanostructure in their fully dense products.<sup>63</sup> SPS has been used to make isotropic nanostructured Nd-Fe-B magnets.<sup>64</sup> Near theoretical density has been achieved. Although SPS method can keep the nanostructure of the feedstock powders prepared using the melt spinning method, it lacks the means to install textures and can only produce isotropic nanocrystalline magnet. Energy products as high as 16 MGOe has been demonstrated. SPS method was also used to make anisotropic Nd-Fe-B and Nd-Co-Ga-Fe-B magnets.<sup>65,66</sup> The feedstock was jet-milled powder about 5  $\mu\text{m}$  in diameter. Before the SPS process, the single crystal powders were orientated in a magnetic field of 2.0 T and pressed with light pressure after they have been enclosed in a graphite mold. The powder retained their alignment and an energy product of 30 MGOe was achieved.<sup>65</sup> It is interesting that the SPS-process Nd-Fe-B magnet exhibited fine and uniform grain size and the distribution of the Nd-rich phase was heterogeneous. SPS method was also used to fabricate exchange-coupled nanocomposite of Nd-Fe-B coated with Fe-Co nanoparticles. Single phase magnetic behavior and enhanced remanence were observed, and the obtained texture was relatively weak ( $M_r$  7 kG).<sup>67</sup>

## **Shock Compaction**

Conventional magnet fabrication methods such as sintering and hot deformation are not applicable for making bulk magnets when feedstock powders are chemically unstable at the sintering temperature. For example, Sm-Fe-N will decompose into SmN and  $\alpha$ -Fe once temperature exceeds 500–600°C.<sup>68</sup> Shock compaction exploits an advantageous combination of parameters: short time (< 1 ms), high stress (> 4 GPa), and low temperature (< 400°C), making it possible to attain bulk magnets of Sm-Fe-N with 2–10% porosity without any phase decomposition.<sup>69,70</sup> Chiba et al.<sup>71</sup> used explosive consolidation under cold state and obtained fully dense magnet  $\text{Sm}_2\text{Fe}_{17}\text{N}_x$  compact with 23.8 MGOe. Similarly,  $\alpha''$ - $\text{Fe}_{16}\text{N}_2$  has a low decomposition temperature (about 222°C).<sup>72</sup> Shock compaction was used to consolidate  $\alpha''$ - $\text{Fe}_{16}\text{N}_2$  powder. In one case, isotropic bulk magnets with over 90% of theoretical density were obtained without decomposition.<sup>73</sup> Minor texture formation was observed. But in another case,  $\alpha''$ - $\text{Fe}_{16}\text{N}_2$  powders were decomposed during the

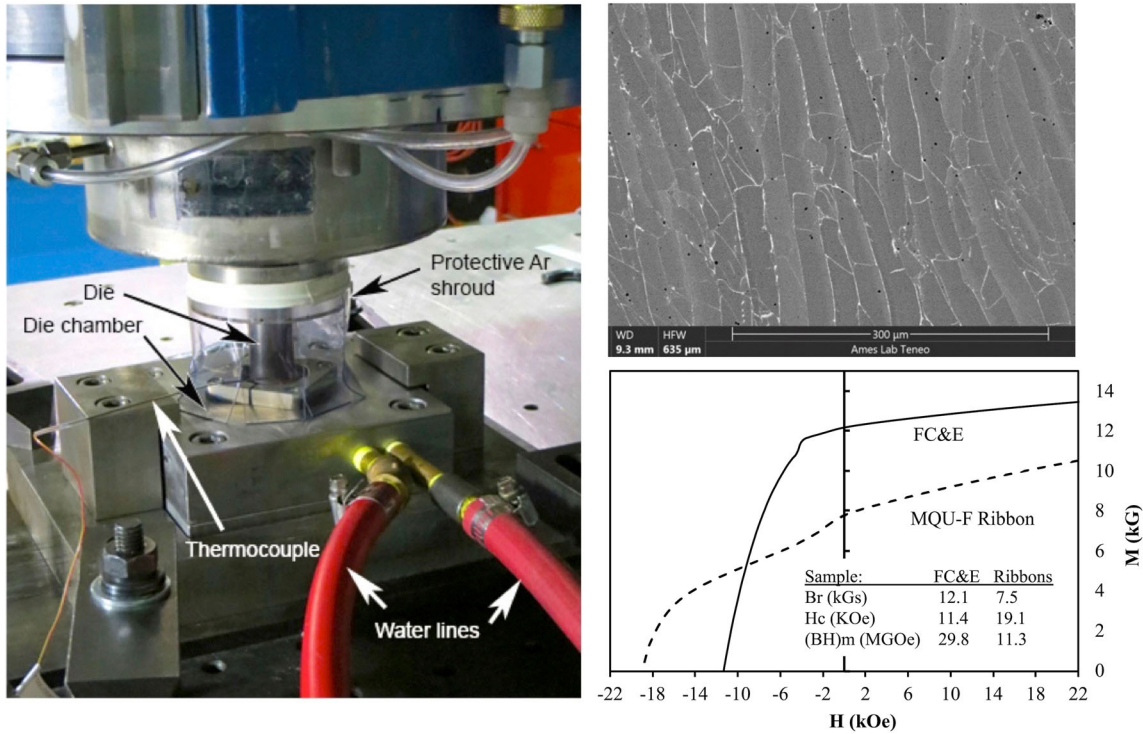


Fig. 3. Picture of a friction consolidation setup. SEM micrographs of friction consolidated disc area, precursor to ring extrusion in sample made from a Nd-Fe-B (MQU-F). And M-H loops of the feedstock and consolidated bulk magnet.

consolidation due to a combination of thermal effects associated with dynamic void collapse and plastic deformation.<sup>74</sup> Shock compaction was also used to consolidate Nd-Fe-B powder. Both decomposition and amorphization of Nd-Fe-B powders were observed.<sup>75</sup>

The shock consolidation process can be classified into four modes: particle sliding, melting, deformation, and hydrodynamic flow. In the sliding mode, the smaller particles move at high velocity and past the large ones to reach the cavity area.<sup>76</sup> The larger particles may deform locally at their boundaries. In the melting mode, particles melt and re-solidify at their boundaries, especially at triple point junctions. The pressure applied is proportional to the energy required for particle surface melting and should be kept on for a minimum duration to allow the molten layer to solidify. In the deformation mode, the void area is filled by the plastically deformed surroundings. Good compacts can be obtained with no evidence of interparticle melting or structural modification, showing that deformation could be the main mechanism for consolidation and melting is not a necessary condition.<sup>77</sup> In the hydrodynamic mode, the particle boundaries disappeared near points of contact of three particles. A large amount of heat was generated due to the localized severe deformation where shear stresses far exceed the yield stress and exceed even the shear modulus.

Bonding occurs by melting at the boundary. It can also occur by hydrodynamic flow, which is a better way for bonding. Materials with low yield stress and

hardness such as nickel or copper may be well compacted and well bonded; but hard materials such as superalloy powders, metal carbides, or ceramics may be well compacted but may not be bonded. Shock compaction creates dislocations and defects. They may enhance the bonding strength but will also reduce the bonding toughness. A brittle bonding is vulnerable to the release wave that immediately following the initial shock wave. A solution to shock hardening is to heat up the compact before shock compaction, so that less defects are formed near the contact surface and the formed defects can be annealed out. In addition, metal powders are typically covered with oxides, hydroxides or nitrides. They are the source of defects and must be removed before compaction.

Shock waves can be generated by explosives, gas guns, lasers, and pulsed (dynamic) magnetic fields. The explosive compaction setup consists of a cylindrical container surrounded by a proper type and amount of explosives. If applied pressure is high enough, a liquid phase sintering process can be achieved.<sup>78</sup> Gas guns are suitable for studying materials under high strain rates. Gas gun systems are extensively instrumented with sensors, allowing repeatable studies of material's responses to shock impaction.<sup>79–83</sup>

Magnetic forces can be used for high-rate metal forming and near net shape powder compaction.<sup>84–86</sup> The basic principle of the magnetic compaction process is similar to the electromagnetic rail-guns.<sup>87,88</sup> A conductive container filled with



powders is placed in the bore of a coil. When pulsed with a high current, the coil produces a high magnetic field, which in turn induces strong currents in the container. The induced current interacts with the high magnetic field producing an inwardly acting magnetic force that collapses the tube. The powders are compacted to near full density (95–97%) in less than one millisecond. The process is suited to produce net-shape parts with cylindrical symmetry, thin-walled tubes, high aspect ratio components and parts with internal features. Magnetic shock compaction was used to develop high-performance magnets. It has been demonstrated that the compacted bonded Nd-Fe-B magnets exhibit a 15–20% increase in energy product due to higher density relative to conventionally processed magnets.<sup>89</sup> However, the process is expensive and slow.

### Thermomagnetic Processing

Thermomagnetic processing, or the application of magnetic fields during heat treatment, has been demonstrated to affect both thermodynamic phase equilibria<sup>90,91</sup> and kinetic behavior,<sup>92,93</sup> leading to the potential for microstructure manipulation, thus, the control of magnetic properties in magnetic materials.<sup>94</sup> The effect of applied magnetic fields on thermodynamic equilibria is understood theoretically through the magnetic moment component of Gibbs free energy, where the difference in free energy is a function of the difference in magnetization of the two phases over the range of an applied field.<sup>95</sup> Naturally, this effect is greater for two phases with different magnetic responses. A complicating effect during heat treatment occurs when the Curie temperature is surpassed and phases become paramagnetic, limiting the thermodynamic effect of the applied field.

Magnetic fields significantly affect nucleation of metallic materials upon solidification and solid-state reactions. The interaction between paramagnetic materials and the applied field has important implications for magnet processing as magnet materials will be in a paramagnetic state at temperature around solidification. There is an absence of evidence to show that nuclei form initially in a textured manner; however, crystallographic texture and magnetic alignment can occur subsequent to nucleation events<sup>96–98</sup> or during subsequent processing.<sup>99</sup> In the Nd-Fe-B system, 2:14:1 phase crystallites form in the melt and rotate, preferentially aligning the *c*-axis in the applied field direction, though this alignment breaks down above 1100°C, likely due to crystallite sizes below that which the field effectively interacts.

Solid-state nucleation from a parent phase or amorphous state are important processes to understand for the processing of magnet materials. These nuclei, unlike those that form from a liquid state, are locked into an orientation after forming. In

alnico, application of the magnetic field assists with enhanced crystallographic texturing. This effect is further enhanced by starting with a directionally solidified parent phase which displays a preferential growth direction. An advantage that alnico possesses is the finely scaled spinodal decomposition that forms the microstructure and emergent extrinsic magnetic properties. In the Nd-Fe-B system, Rietveld refinements revealed a degree of alignment of the 2:14:1 phase after annealing in a 10 T fields.<sup>100</sup> In the case of melt-spun Mn-Bi based alloy, a short annealing at 265–300°C in a moderate magnetic field of 3 T increases the fraction of the desired  $\alpha$  MnBi phase to 97–98% and aligns the *c* axes of the  $\alpha$  crystallites. A maximum energy product  $(BH)_{\max}$  of 11.5 MG Oe and an intrinsic coercivity 5.6 kOe have been obtained in a MnBi based magnet.<sup>101,102</sup>

Perhaps the most consistently observed phenomenon observed when applying strong magnetic fields during annealing treatments is a refinement of the microstructure when compared with no-field annealing. Exploration into thermomagnetic processing of ferrous alloys have the greatest body of literature demonstrating this effect,<sup>95,103,104</sup> though several magnet material systems have demonstrated it as well, including Nd-Fe-B<sup>105,106</sup> and Pr-Co-B<sup>107</sup> systems. The mechanisms underlying this effect are not well understood due to the interplay of thermodynamic and kinetic processes. For the Nd-Fe-B system, heating near-amorphous ribbons in magnetic fields of 0 T to 9 T revealed an unchanged crystallization temperature, but slower growth at a given annealing temperature as the applied field increased.<sup>105</sup> The Pr-Co-B system was impacted by thermodynamic effects due to the stabilization of the high-moment, ferromagnetic 2:17 phase.<sup>107</sup> While the microstructure was significantly refined as the field increased (Fig. 4), the volume fraction of the magnetically soft 2:17 phase also increased resulting in reduced coercivity despite a finer structure.

Ultimately, the primary properties of interest for permanent magnet applications are coercivity and remanence, both of which can be controlled with the application of high magnetic fields. Permanent magnet systems Nd-Fe-B have been shown to respond well to thermomagnetic processing. Improved coercivity in these systems generally develops due to microstructural refinement.<sup>100,105,108</sup> Limited magnetic alignment has been observed in the annealing studies of these particular alloys as their magnetic anisotropy is linked to their crystal structure, which is nearly locked in its orientation by the starting condition prior to annealing. Though much work is still needed to further elucidate the mechanisms behind the observed experimental effects, there is much promise in the area of thermomagnetic processing of magnet materials.

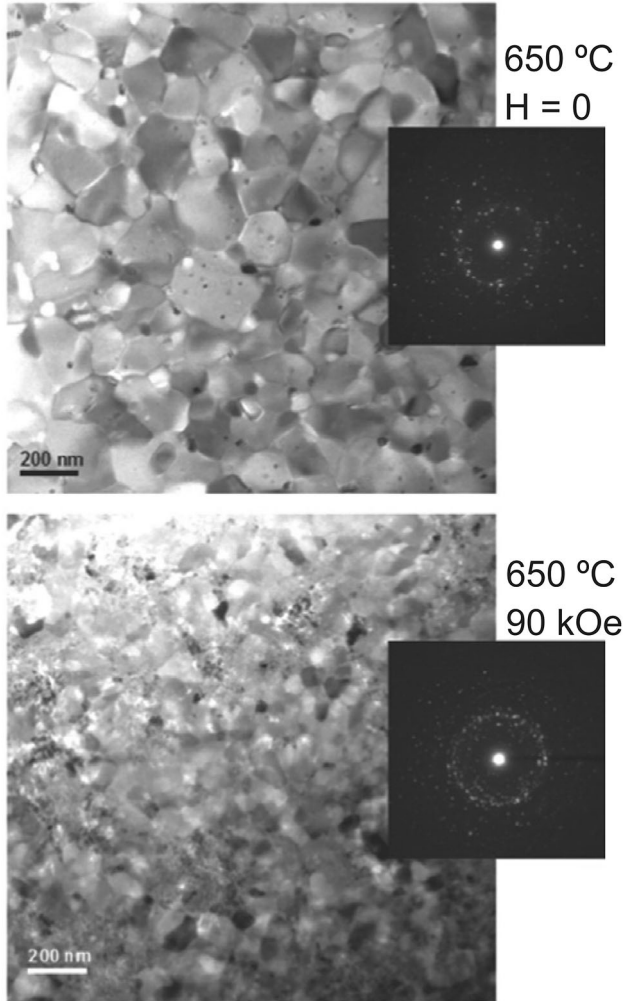


Fig. 4. Pr-Co-B ribbons annealed at 650°C for 5 min under applied fields of 0 kOe (top) and 90 kOe (bottom) with selected area diffraction insets showing a nanocrystalline structure. Reprinted from Ref. 107 with permission from Elsevier.

### Comparison of Less Common and Novel Magnet Fabrication Processes

One way to quickly evaluate the progress of these less common and novel magnet fabrication processes discussed in the previous sections is to compare the achieved  $(BH)_{\max}$  and the theoretical maximum energy product ( $M_s^2/4$ ). Table I summarized these values. In the table, the achieved  $(BH)_{\max}$  for the cold spray method was estimated based on the B-H curve in Ref. 32; the  $M_s$  of the feedstock powder (9 kG) used by the directed energy deposition method was measured by Dr. McCall; the achieved  $(BH)_{\max}$  for the torsion extrusion method was estimated based on the M-H curves in Ref. 58. The feedstock  $M_s$  for the spark plasma sintering method was estimated based on the composition reported in Ref. 65. The thermomagnetic processing aims at improving coercivity of the sintered bulk magnet. Instead of listing the  $M_s^2/4$  value of the feedstock powder, the  $(BH)_{\max}$  of the bulk magnet before magnetic annealing is listed.

### RECYCLING OF RARE EARTH ELEMENTS FROM PERMANENT MAGNETS

The US Department of Energy identified recycling and reuse as one of the strategies for addressing materials criticality.<sup>109</sup> Similar strategy was then adopted by the European Commission<sup>110</sup> and Japanese Ministry of Trade.<sup>111</sup> Recycling was mainly intended to be a secondary source for REEs, compared to materials from natural sources. However, recycling of REEs is not trivial—a reason for which it is still minimally practiced. To advance REEs recycling into commercial practice, it must be economically profitable. Ferron and Henry have identified that the economic values of recycling need to be balanced with other ‘soft’ incentives including resource independence, sustainability and stewardship.<sup>112</sup> Nlebedim and King have previously recommended a flowchart to guide that decision.<sup>113</sup> Also, Habib has recommended a product classification approach in which the decision to progress from reuse to repair and to recovery of critical elements will depend on whether a product falls within one of three class levels.<sup>114</sup>

#### Direct Reuse of REE Magnets

An efficient way to recycle REEs in permanent magnets is to directly reuse the magnets with no additional reprocessing applied.<sup>115–117</sup> It eliminates the need for remanufacturing and elemental recovery. Extraction of magnets for reuse is challenging, depending on the type of device and where in the device the magnets are located. For instance, magnets from internal permanent magnet electrical machines may be less readily accessible compared to surface mounted machine topologies. Also, magnets of larger sizes will be easier to extract, while small magnets, such as those used in cell phones, are difficult to efficiently harvest.<sup>114,118</sup> Many of the magnet extraction technologies are manual. Although automated processes for harvesting Nd-Fe-B magnets from devices like HDDs have been proposed<sup>119–121</sup> there are no automated processes for verifying the mechanical integrity of the magnets to ensure that they are suitable for reuse. A potential research direction will be developing a nondestructive evaluation technique for quick assessment of magnets prior to reuse.

One of the biggest challenges with direct reuse is dismantling of the magnets, as can be seen from the European MORE-project.<sup>122</sup> Dismantling involves demagnetization of the magnets to improve handling and debonding from the adhesives that are typically applied to hold the magnets in place. For direct reuse, both demagnetization and debonding processes need to be performed in ways that retain the integrity of the protective coatings on the magnets. Högborg et al.<sup>123</sup> have investigated the effects of thermal demagnetization on the integrity of the coatings on Nd-Fe-B magnets. Heating magnets coated with Zn, Epoxy, Ni-Cu-Ni, and Ni-

**Table I. Key magnet properties prepared by less common and novel magnet manufacturing methods**

| Magnet process                     | fabrication | Feedstock Materials                         | Achieved $(BH)_{\max}$ (MGOe)  | Feedstock $M_s^{2/4}$ (MGOe)   | References |
|------------------------------------|-------------|---|--------------------------------|--------------------------------|------------|
| 3D printing of bonded magnet       |             | Nd-Fe-B/binder                              | 19.9                           | 24.0                           | 21         |
| Directed energy deposition         |             | Nd-Pr-Zr-Ti-Co-Fe-B atomized powder (MQP-S) | 5.7                            | 20.3                           | 26         |
| Cold spray                         |             | Nd-Fe-B (MQFP-B) and Al powder mix          | 3.5                            | 10.6                           | 32         |
| Die upset and backward extrusion   |             | Nd-Fe-B jetmill powder                      | 53.0                           | 55.5                           | 40         |
| Equal channel angular extrusion    |             | Nd-Fe-Co-B-Ga meltspun powder (MQU-F)       | 19.5                           | 49.0                           | 53         |
| Torsion extrusion                  |             | Nd-Fe-B ingot                               | 12.3                           | 33.6                           | 58         |
| Friction consolidation & extrusion |             | Nd-Fe-B jetmill powder                      | 29.8                           | 45.6                           | 59         |
| Spark plasma sintering             |             | Nd-Dy-Fe-Co-B-Al jetmill powder             | 30.2                           | 39.1                           | 65         |
| Shock compaction                   |             | Sm-Fe-N powder                              | 23.8                           | 56.3                           | 71         |
| Thermomagnetic processing          |             | Nd-Fe-B (N40) sintered bulk                 | 39.1<br>( $H_c \sim 21.6$ kOe) | 39.1<br>( $H_c \sim 19.4$ kOe) | 108        |

Cu+Epoxy to 350°C in nitrogen atmosphere was found not to cause any degradation in the hard magnetic properties.

Debonding is performed using chemicals like NaOH, acetone or dimethylformamide, mineral acids, methylene chloride and dimethyl sulfoxide.<sup>117,124,125</sup> Those chemicals can have negative health and environmental impacts. Also, the process of debonding the magnets may compromise the integrity of the coating material and may necessitate re-coating of the magnets. Heating the magnet assembly can carbonize the adhesive material<sup>119</sup> and will require polishing to remove the carbonized material from the magnet.<sup>126</sup> Such additional polishing step may impact the economics benefits of direct reuse recycling. A possible research direction is the development of bonding agents that enable strong attachment of magnets in devices but easy dismantling for reuse.

### Reprocessing/Remanufacturing/Refurbishing of Permanent Magnets

Scrap magnets are those fractured during manufacturing and post-manufacturing processes, including magnets damaged when harvested from devices and those damaged by harsh environments. To make permanent magnet recycling economically viable, the number of processing steps prior to reinsertion into the supply chain needs to be minimized. Rated performance such as torque or power may be achieved by directly reusing a magnet without reprocessing it (e.g. reshaping), but it can lead to degrading other parameters, compared to using an appropriately shaped magnet.

Walton et al.<sup>127</sup> have demonstrated that magnets in waste electronic devices can be harvested by exposing the device to hydrogen pressure such that hydrogen is absorbed into the microstructure of Nd-Fe-B magnets leading to decrepitation into powder. Afterwards, such magnet powder can be used as a feedstock for producing new sintered magnets.<sup>128</sup> One of the biggest merits of this process is that it employs a step typical for magnet production, i.e. hydrogen decrepitation. It also serves as a means for removing the protective plating on Nd-Fe-B magnets by simple sieving operations. Properties of the magnets remade with such powders can be enhanced by the use of REE-rich additives.<sup>129–131</sup> Nevertheless, since the surface of the magnets must be exposed to hydrogen, this process is likely most applicable to magnets that have been extracted and fractured to allow hydrogen decrepitation process. It may also be limited if the magnet is covered with an oxide layer that restricts permeation of hydrogen into the magnet. Also, the process will mostly be applicable to Nd-Fe-B type of magnets, hence the need for predetermination of the magnet type.

Another approach to reprocessing waste sintered magnets is to convert them to powders for bonded magnets application. Li et al.<sup>132</sup> have reported on mechanical crushing and hydrogen decrepitation as approaches for reprocessing waste sintered magnets into bonded magnets. They found that the powders recycled via the hydrogen decrepitation performed better than the powder recycled via mechanical milling, although the remanence and coercivity degraded for both methods—with coercivity degrading the most. Gandha et al.<sup>18</sup> reported on recycling waste bonded magnets by pulverizing thermoplastic bonded magnets in liquid nitrogen and then warm-



**Table II. Possible future directions for developing novel magnet manufacturing methods**

| Objective   | Challenges  | Approaches  |
|---|---|---|
| Sinter fine grain bulk Nd-Fe-B magnet with high coercivity  | Nd-Fe-B powders finer than 3 $\mu\text{m}$ are pyrophoric. They are expensive to make and handle  | A novel passivation technique allowing the powder to be handled with existing setups  |
| Hot deform anisotropic bulk Nd-Fe-B magnet with nanograins and near-net-shape cross-section and high coercivity | Texture is less than ideal because higher deformation temperature will cause grain growth and lower coercivity. The back-to-back hot press and hot deformation process is expensive | A novel hot work process that can combine hot-press and hot deformation in one run. And a new chemistry that allow plastic deformation at lower temperature |
| Make anisotropic bulk magnet directly from Nd-Fe-B ingot  | Torsional extrusion and friction extrusion both refine grain size, but the recrystallized grains are not well aligned   | A novel far-from-equilibrium process that provide the thermal, mechanical, and magnetic boundary conditions for directional recrystallization               |
| Make bulk anisotropic exchange-coupled nanocomposite magnet   | Hard/soft phases have to be less than 100/10 nm and hard phase has to be textured. The nano size soft phase will grow at sintering temperature causing decoupling                   | A novel method that can refine the Sm-Co grains while align them for making Sm-Co-Fe nanocomposite  |
| Make anisotropic bulk magnet of Sm-Fe-N or $\text{Fe}_{16}\text{N}_2$   | Nitride decompose below sintering temperature   | A novel far-from-equilibrium process that can densify the nitride without decomposition   |
| 3D-Print fully dense anisotropic magnet   | Laser or ebeam melting cannot create nano grains or textured microstructures with well distributed intergranular phase  | A modified friction welding process   |

compacting the powders to remake bonded magnets. The approach used by the authors yielded magnets having  $B_r$ ,  $H_c$ , and  $(\text{BH})_{\text{max}}$  in the range 96–104%, 90–96% and 86–100%, respectively, compared to the waste bonded magnet being recycled. The possibility to remake magnets with properties matching or exceeding the original magnets without the use of additives, is interesting. However, this method is not suitable for bonded magnets made with thermosets.

### Elemental Recovery

When magnets cannot be directly reused or reprocessed/remanufactured/refurbished, elemental recovery is the only available option to recycle REEs. As an example, elemental recovery is the main option available for recycling REEs from HDDs typically shredded at end-of-life for information security. Elemental recovery requires separating the REEs and other valuable elements (e.g. Co) in the magnets, via two key approaches: pyrometallurgy and hydrometallurgy.<sup>113,119</sup> Pyrometallurgical methods can recover materials as metals, instead of oxides, but are limited by large energy consumption and significant solid waste generation.<sup>112</sup> Hydrometallurgical methods can be more efficient but recover materials as oxides and use high volumes of mineral acids and other harsh chemicals,<sup>133,134</sup> which results in the generation of acid-contaminated wastes. This creates obvious

environmental, health and safety concerns. Different pyrometallurgical and hydrometallurgical methods have been reported in the literature and will not be covered in this review. This includes an acid-free dissolution hydrometallurgical process that mitigates the stated environmental, health and safety concerns.<sup>135</sup>

### FUTURE DIRECTIONS

Magnet manufacturers are always working on improving the manufacturing process for lower variability, less waste, and higher efficiency. Most of the processes are mature and well optimized for maximum profitability. The future of the magnet industry lies in new chemistries and the manufacturing process that can enable them. Table II lists example directions that may create big impacts in the magnet industry.

### SUMMARY

Due to their high energy density  $(\text{BH})_{\text{max}}$ , rare earth permanent magnets play critical roles in many advanced technologies indispensable for the transition to a clean energy economy. Rare-earth magnets are important not only for hybrid and electric vehicles, but also for applications where compact, high-efficiency motors with high power densities are essential, such as for drones and aerospace needs. For EVs, the high efficiency achieved by permanent magnet motors allows for

increased range while reducing energy storage requirements. The rapid growth in demand for RE permanent magnets is placing increased stress on the availability of key elements, particularly Nd, Pr, and Dy, which will present a bottleneck in transitioning towards a net-zero carbon economy. While increasing sources is one mitigation strategy, improvements to manufacturing processes can aid in ameliorating this challenge of meeting the demand. This may take the form of better materials efficiency—reducing losses due to waste. Here, advanced manufacturing techniques may help achieve these goals, where near-net-shape fabrication can reduce both materials losses and total machining costs. Reductions in materials intensity—the quantity of materials needed—is possible through precision synthesis, such as functional grading of Dy, where this very expensive metal may be selectively deployed to regions of the magnets where it is essential. Similarly, replacing some fraction of Nd with less critical RE such as Ce and La may provide value if the necessary magnetic properties can be retained. Finally, tighter control of processing conditions can minimize the production variation from batch-to-batch, but also within individual batches, which can arise due to local temperature gradients in furnaces. This can ensure that a higher fraction of RE magnets meet the rigorous specifications needed for a cleaner, greener economy.

### ACKNOWLEDGEMENTS

This work is supported by the Critical Materials Institute (CMI), an Energy Innovation Hub funded by the US Department of Energy (DOE), Office of Energy Efficiency and Renewable Energy, Advanced Manufacturing Office. Ames Laboratory is operated for the U.S. Department of Energy by Iowa State University of Science and Technology under Contract No. DE-AC02-07CH11358. Work at LLNL and ORNL performed under Contracts DE-AC52-07NA27344 and DE-AC05-00OR22725, respectively. On behalf of all authors, the corresponding author states that there is no conflict of interest.

### OPEN ACCESS

This article is licensed under a Creative Commons Attribution 4.0 International License, which permits use, sharing, adaptation, distribution and reproduction in any medium or format, as long as you give appropriate credit to the original author(s) and the source, provide a link to the Creative Commons licence, and indicate if changes were made. The images or other third party material in this article are included in the article's Creative Commons licence, unless indicated otherwise in a credit line to the material. If material is not included in the article's Creative Commons licence and your intended use is not permitted by statutory regulation or exceeds the permitted use, you will need to obtain permission directly from the copy-

right holder. To view a copy of this licence, visit <http://creativecommons.org/licenses/by/4.0/>.

### REFERENCES

1. "Neodymium Iron Boron Magnets" (Arnold Magnetics), <https://www.arnoldmagnetics.com/products/neodymium-iron-boron-magnets/>, Accessed from 18 Dec 2021.
2. "Neodymium Magnets Summary", TDK, <https://product.tdk.com/en/products/magnet/magnet/neodymium/index.html>, Accessed from 18 Dec 2021.
3. "Rare-Earth Permanent Magnets VACODYM-VACOMAX", (Vacuumschmelze), <https://vacuumschmelze.com/products/Permanent-Magnets/Magnet-Assemblies>.
4. Sintered Nd-Fe-B magnets, (Zhong Ke San Huan), <https://en.san-huan.com.cn/Product/Product1>.
5. "Cast Alnico catalog" (Arnold Magnetics), <https://www.arnoldmagnetics.com/products/alnico-magnets/>, Accessed from 18 Dec 2021.
6. "Ferrite Magnets FB Series Magnetic Characteristics Distribution Chart", (TDK), <https://product.tdk.com/en/products/selectionguide/ferrite-magnet.html>.
7. J. Ormerod and S. Constantinides, *J. Appl. Phys.* 81, 4816. (1997).
8. M. Przybylski, B. Ślusarek, and J. Gromek, in *The XIX International Conference on Electrical Machines*, 1 (2010).
9. L. Ferraris, F. Franchini, and E. Poskovic, in *IEEE 26th International Symposium on Industrial Electronics*, 374 (2017).
10. M.P. Paranthaman, V. Yildirim, T.N. Lamichhane, B.A. Begley, B.K. Post, A.A. Hassen, B.C. Sales, K. Gandha, and I.C. Nlebedim, *Materials* 13, 3319 (2020).
11. E. Agamloh, A. von Jouanne, and A. Yokochi, *Machines* 8, 20 (2020).
12. M.P. Paranthaman, C.S. Shafer, A.M. Elliott, D.H. Sittel, M.A. McGuire, R.M. Springfield, J. Martin, R. Fredette, and J. Ormerod, *JOM* 68, 1978 (2016).
13. L. Li, B. Post, V. Kunc, A.M. Elliott, and M.P. Paranthaman, *Scr. Mater.* 135, 100 (2017).
14. M.P. Paranthaman, I.C. Nlebedim, F. Johnson, and S.K. McCall, *Mater. Matters* 11, 4 (2016).
15. L. Li, A. Tirado, B.S. Conner, M. Chi, A.M. Elliott, O. Rios, H. Zhou, and M.P. Paranthaman, *J. Magn. Magn. Mater.* 438, 163 (2017).
16. L. Li, A. Tirado, I.C. Nlebedim, O. Rios, B. Post, V. Kunc, R.R. Lowden, E. Lara-Curzio, R. Fredette, J. Ormerod, T.A. Lograsso, and M.P. Paranthaman, *Sci. Rep.* 6, 1 (2016).
17. L. Li, K. Jones, B. Sales, J.L. Pries, I.C. Nlebedim, K. Jin, H. Bei, B.K. Post, M.S. Kesler, O. Rios, V. Kunc, R. Fredette, J. Ormerod, A. Williams, T.A. Lograsso, and M.P. Paranthaman, *Addit. Manuf.* 21, 495 (2018).
18. K. Gandha, G. Ouyang, S. Gupta, V. Kunc, M.P. Paranthaman, and I.C. Nlebedim, *Waste Manag.* 90, 94 (2019).
19. I.C. Nlebedim, H. Ucar, C.B. Hatter, R.W. McCallum, S.K. McCall, M.J. Kramer, and M.P. Paranthaman, *J. Magn. Magn. Mater.* 422, 168 (2017).
20. K. Gandha, L. Li, I.C. Nlebedim, B.K. Post, V. Kunc, B.C. Sales, J. Bell, and M.P. Paranthaman, *J. Magn. Magn. Mater.* 467, 8 (2018).
21. K. Gandha, I.C. Nlebedim, V. Kunc, E. Lara-Curzio, R. Fredette, and M.P. Paranthaman, *Scr. Mater.* 183, 91 (2020).
22. A. Sarkar, M.A. Somashekara, M.P. Paranthaman, M. Kramer, C. Haase, and I.C. Nlebedim, *Addit. Manuf.* 34, 101289 (2020).
23. N. Sridharan, E. Cakmak, F.A. List, H. Ucar, S. Constantinides, S.S. Babu, S.K. McCall, and M.P. Paranthaman, *J. Mater. Sci.* 53, 8619 (2018).
24. J. Jacimovic, *Sustainable Industrial Processing Summit SIPS2019*, vol 3. (Flogen Star OUTREACH, Montreal, Canada, 2019), pp 50–51.
25. C. Huber, H. Sepehri-Amin, M. Goertler, M. Groenefeld, I. Teliban, K. Hono, and D. Suess, *Acta Mater.* 172, 66 (2019).

26. J. Jacimovic, F. Binda, L.G. Herrmann, F. Greuter, J. Genta, M. Calvo, T. Tomse, and R.A. Simon, *Adv. Eng. Mater.* 19, 1700098 (2017).
27. E.M.H. White, A.G. Kassen, E. Simsek, W. Tang, R.T. Ott, and I.E. Anderson, *IEEE Trans. Magn.* 53, 1 (2017).
28. E. White, E. Rinko, T. Prost, T. Horn, C. Ledford, C. Rock, and I. Anderson, *Appl. Sci.* 9, 4843 (2019).
29. S. Yin, P. Cavaliere, B. Aldwell, R. Jenkins, H. Liao, W. Li, and R. Lupoi, *Addit. Manuf.* 21, 628 (2018).
30. A.A. Baker, R. Thuss, N. Woollett, A. Maich, E. Stavrou, S.K. McCall, and H.B. Radousky, *JOM* 72, 2853 (2020).
31. F. Bernier and J.M. Lamarre, in *Québec, a Leader in Transportation Electrification: 29th World Electric Vehicle Symposium and Exhibition (EVS29)* (Ministère des transports, de la mobilité durable et de l'électrification des transports, Montréal, 2016), p. 9.
32. J.M. Lamarre and F. Bernier, *J. Therm. Spray Technol.* 28, 1709 (2019).
33. W.F. Li, T. Ohkubo, K. Hono, and M. Sagawa, *J. Magn. Mater.* 321, 1100 (2009).
34. H. Sepehri-Amin, Y. Une, T. Ohkubo, K. Hono, and M. Sagawa, *Scr. Mater.* 65, 396 (2011).
35. R.K. Mishra, *J. Appl. Phys.* 62, 967 (1987).
36. O. Gutfleisch, A. Kirchner, W. Grünberger, D. Hinz, H. Nagel, P. Thompson, J.N. Chapman, K.H. Müller, L. Schultz, and I.R. Harris, *J. Phys. D Appl. Phys.* 31, 807 (1998).
37. L. Li and C.D. Graham, *IEEE Trans. Magn.* 28, 2130 (1992).
38. K.G. Knoch, B. Reinsch, and G. Petzow, *Z. Fuer Metallkunde* 85 (5), 350 (1994).
39. A. Kirchner, J. Thomas, O. Gutfleisch, D. Hinz, K.H. Müller, and L. Schultz, *J. Alloys Compd.* 365, 286 (2004).
40. Z. Wang, J. Ju, J. Wang, W. Yin, R. Chen, M. Li, C. Jin, X. Tang, D. Lee, and A. Yan, *Sci. Rep.* 6, 1 (2016).
41. D. Hinz, A. Kirchner, D.N. Brown, B.M. Ma, and O. Gutfleisch, *J. Mater. Process. Technol.* 135, 358 (2003).
42. J.J. Croat, *IEEE Trans. Magn.* 25, 3550 (1989).
43. W. Grünberger, D. Hinz, A. Kirchner, K.H. Müller, and L. Schultz, *J. Alloys Compd.* 257, 293 (1997).
44. "Radially Oriented, Anisotropic Nd-Fe-B Ring Magnets (NEOQUENCH-DR)" (DAIDO Electronics) [http://www.daido-electronics.co.jp/english/product/neoquench\\_dr/index.html](http://www.daido-electronics.co.jp/english/product/neoquench_dr/index.html). Accessed from 5 Jun 2021.
45. V.M. Segal, V.I. Reznikov, A.E. Dorbryshevshiy, and V.I. Kopylov, *Russ. Metal. (METALLY)* 1, 99 (1981).
46. V.M. Segal, *Mater. Sci. Eng. A* 197, 157 (1995).
47. S. Ferrasse, K.T. Hartwig, R.E. Goforth, and V.M. Segal, *Metall. Mater. Trans. A* 28, 1047 (1997).
48. K. Nakashima, Z. Horita, M. Nemoto, and T.G. Langdon, *Acta Mater.* 46, 1589 (1998).
49. M. Moss, R. Lapovok, and C.J. Bettles, *JOM* 59, 54 (2007).
50. J.A. Hanna and I. Baker, *Mater. Sci. Eng. A* 536, 24 (2012).
51. A. Chaturvedi, R. Yaqub, and I. Baker, *Metals* 4, 20 (2014).
52. T. Ohtani, N. Kato, S. Kojima, K. Kojima, Y. Sakamoto, I. Konno, M. Tsukahara, and T. Kubo, *IEEE Trans. Magn.* 13, 1328 (1977).
53. E. Onal, R. Lapovok, H. Kishimoto, A. Kato, C.H.J. Davies, and K. Suzuki, *IEEE Trans. Magn.* 52, 1 (2016).
54. B. Omranpour, Y. Ivanisenko, R. Kulagin, L. Kommel, E. Garcia Sanchez, D. Nugmanov, T. Scherer, A. Heczal, and J. Gubicza, *Mater. Sci. Eng. A* 762, 138074 (2019).
55. Y. Ivanisenko, R. Kulagin, V. Fedorov, A. Mazilkin, T. Scherer, B. Baretzky, and H. Hahn, *Mater. Sci. Eng. A* 664, 247 (2016).
56. R. Kulagin, Y. Beygelzimer, Y. Estrin, Y. Ivanisenko, B. Baretzky, and H. Hahn, *Metals* 9, 306 (2019).
57. S. Mizunuma, *Mater. Sci. Forum* 503–504, 185 (2006).
58. B.B. Straumal, A.A. Mazilkin, S.G. Protasova, D.V. Gunderov, G.A. López, and B. Baretzky, *Mater. Lett.* 161, 735 (2015).
59. M. Marinescu, J. Cui, G. Grant, S. Jana, J. Darsell, M. J. Kramer, and J. Liu, in *23rd International Workshop on Rare Earth and Future Permanent Magnets and Their Applications (REPM2014)* (Curran Associates, Inc., Annapolis, Maryland, 2014), p. 203.
60. W.M. Thomas, E.D. Nicholas, and S.B. Jones, US5262123A (1993).
61. J. Cui, G.J. Grant, S. Jana, Y. Hovanski, and C.A. Laverder, US10109418B2 (2 May 2013).
62. K. Sairam, J.K. Sonber, T.S.R.C. Murthy, C. Subramanian, R.K. Fotedar, P. Nanekar, and R.C. Hubli, *Int. J. Refract. Met. Hard Mater.* 42, 185 (2014).
63. M. Tokita, in *NEDO International Symposium on Functionally Graded Materials* 23 (1999).
64. T. Tomše, J. Jaćimović, L. Herrmann, F. Greuter, R. Simon, S. Tekavec, J.M. Dubois, and S. Kobe, *J. Alloys Compd.* 744, 132 (2018).
65. M. Yue, J. Zhang, Y. Xiao, G. Wang, and T. Li, *IEEE Trans. Magn.* 39, 3551 (2003).
66. Z.W. Liu, H.Y. Huang, X.X. Gao, H.Y. Yu, X.C. Zhong, J. Zhu, and D.C. Zeng, *J. Phys. D Appl. Phys.* 44, 025003 (2011).
67. K.P. Su, Z.W. Liu, H.Y. Yu, X.C. Zhong, W.Q. Qiu, and D.C. Zeng, *J. Appl. Phys.* 109, 7 (2011).
68. J.M.D. Coey and H. Sun, *J. Magn. Mater.* 87, 251 (1990).
69. M. Leonowicz, W. Kaszuwara, E. Jezierska, D. Januszewski, G. Mendoza, H.A. Davies, and J. Paszula, *J. Appl. Phys.* 83, 6634 (1998).
70. T. Mashimo, X. Huang, S. Hirose, K. Makita, Y. Kato, S. Mitsudo, and M. Motokawa, *J. Magn. Mater.* 210, 109 (2000).
71. A. Chiba, K. Ooyabu, Y. Morizono, T. Maeda, S. Sugimoto, T. Kozuka, E. Kakimoto, K. Kawahara, and T. Watanabe, *Mats. Sci. Forum.* 449, 1037 (2004).
72. K. Takagi, M. Akada, K. Ozaki, N. Kobayashi, T. Ogawa, Y. Ogata, and M. Takahashi, *J. Appl. Phys.* 115, 103905 (2014).
73. Y. Jiang, J. Liu, P.K. Suri, G. Kennedy, N.N. Thadhani, D.J. Flannigan, and J.P. Wang, *Adv. Eng. Mater.* 18, 1009 (2016).
74. C. Wehrenberg, B. Zande, S. Simizu, R.T. Obermyer, S.G. Sankar, and N. Thadhani, *J. Appl. Phys.* 111, 83522 (2012).
75. C. Wehrenberg, Phase Transformations In Shock Compacted Magnetic Materials (Doctoral dissertation, Georgia Institute of Technology, 2012).
76. H. Matsumoto and K.I. Kondo, *J. Mater. Sci.* 24, 4042 (1989).
77. L.E. Murr, S. Shankar, A.W. Hare, and K.P. Staudhammer, *Scr. Metall.* 17, 1353 (1983).
78. R. Prümmer, *Materwiss. Werkstofftech.* 20, 410 (1989).
79. T.J. Downs, The Development of a Single Stage Light Gas Gun and Velocity Measurement System (Master's thesis, Marquette University, 2006).
80. A.C. Charters, *Int. J. Impact Eng.* 5, 181 (1987).
81. E.J. Workman, Development of New Gun Using Helium Gas for Projectile Acceleration, NMSM/RDD/T70, New Mexico School of Mines, Socorro, NM (1952).
82. L.C. Chhabildas, L. Davison, and Y. Horie, *High-Pressure Shock Compression of Solids VIII* (Springer-Verlag, New York, 2005), pp. 1–35.
83. W.D. Crozier and W. Hume, *J. Appl. Phys.* 28, 892 (1957).
84. M.A. Meyers and L.E. Murr, *Shock Waves and High-Strain-Rate Phenomena in Metals* (Springer Science & Business Media, 1981).
85. W.H. Gourdin, *Prog. Mater. Sci.* 30, 39 (1986).
86. B. Chelluri and J.P. Barber, US5405574A (10 February 1992).
87. L. Xu and Y. Geng, *Appl. Math. Model.* 36, 1465 (2012).
88. S.C. Rashleigh and R.A. Marshall, *J. Appl. Phys.* 49, 2540 (1978).
89. J. Barber, *Met. Powder Rep.* 55, 22 (2000).
90. J.K. Choi, H. Ohtsuka, Y. Xu, and W.Y. Choo, *Scr. Mater.* 43, 221 (2000).
91. H.D. Joo, J.K. Choi, S.U. Kim, N.S. Shin, and Y.M. Koo, *Metall. Mater. Trans. A Phys. Metall. Mater. Sci.* 35A, 1663 (2004).



92. R. Onodera, S. Kimura, K. Watanabe, Y. Yokoyama, A. Makino, and K. Koyama, *Mater. Trans.* 54, 1232 (2013).
93. Z.H.I. Sun, M. Guo, J. Vleugels, O. van der Biest, and B. Blanpain, *Curr. Opin. Solid State Mater. Sci.* 16, 254 (2012).
94. S. Rivoirard, *JOM* 65, 901 (2013).
95. G.M. Ludtka, R.A. Jaramillo, R.A. Kisner, J.B. Wilgen, G. Mackiewicz-Ludtka, D.M. Nicholson, T.R. Watkins, P. Kalu, and R.D. England, *Materials Processing in Magnetic Fields* (World Scientific Pub Co Pte Lt, 2005), pp. 55–65. [https://doi.org/10.1142/9789812701800\\_0007](https://doi.org/10.1142/9789812701800_0007).
96. P. Courtois, R.P. de La Bâthie, and R. Tournier, *J. Magn. Magn. Mater.* 153, 224 (1996).
97. S. Rivoirard, V.M.T.S. Barthém, R. Bres, E. Beaunon, P.E.V. de Miranda, and D. Givord, *J. Appl. Phys.* 104, 43915 (2008).
98. R.F. Tournier and E. Beaunon, *Sci. Technol. Adv. Mater.* 10, 014501 (2009).
99. S. Liesert, D. Fruchart, P. de Rango, S. Rivoirard, J.L. Soubeyroux, R.P. de La Bâthie, and R. Tournier, *J. Alloys Compd.* 262–263, 366 (1997).
100. H. Kato, K. Koyama, and K. Takahashi, *J. Appl. Phys.* 109, 07A726 (2011).
101. A.M. Gabay, G.C. Hadjipanayis, and J. Cui, *J. Alloys Compd.* 822, 153663 (2020).
102. A.M. Gabay, G.C. Hadjipanayis, and J. Cui, *J. Magn. Magn. Mater.* 495, 165860 (2020).
103. J. Li and W. Liu, *J. Magn. Magn. Mater.* 362, 159 (2014).
104. H. Ohtsuka, *Curr. Opin. Solid State Mater. Sci.* 8, 279 (2004).
105. M. Kesler, B. Jensen, L. Zhou, O. Palasyuk, T.-H. Kim, M. Kramer, I. Nlebedim, O. Rios, and M. McGuire, *Magnetochemistry* 5, 16 (2019).
106. B.Z. Cui, C.T. Yu, K. Han, J.P. Liu, H. Garmestani, M.J. Pechan, and H.J. Schneider-Muntau, *J. Appl. Phys.* 97, 10F308 (2005).
107. M.A. McGuire, O. Rios, B.S. Conner, W.G. Carter, M. Huang, K. Sun, O. Palasyuk, B. Jensen, L. Zhou, K. Dennis, I.C. Nlebedim, and M.J. Kramer, *J. Magn. Magn. Mater.* 430, 85 (2017).
108. H. Kato, T. Miyazaki, M. Sagawa, and K. Koyama, *Appl. Phys. Lett.* 84, 4230 (2004).
109. US-DOE, *Critical Materials Strategy* (Washington, DC, 2011). [https://energy.gov/sites/prod/files/DOE\\_CMS2011\\_FINAL\\_Full.pdf](https://energy.gov/sites/prod/files/DOE_CMS2011_FINAL_Full.pdf).
110. European Commission, in *REPORT ON CRITICAL RAW MATERIALS FOR THE EU Report of the Ad Hoc Working Group on Defining Critical Raw Materials* (2014).
111. Y. Inoue and J. Gordon, *Analysis: Japanese Rare Earth Consumers Set up Shop in China*, Reuters, Tokyo, August 12, 2011. <https://www.reuters.com/article/usrareearth-japan/analysis-japanese-rareearth-consumers-set-up-shop-in-chinaidUSTRE77B3TH20110812>.
112. C.J. Ferron and P. Henry, *Can. J. Metall. Mater. Sci.* 54, 388 (2015).
113. I.C. Nlebedim and A.H. King, *JOM* 70, 115 (2018).
114. K. Habib, *J. Clean. Prod.* 230, 90 (2019).
115. S. Hogberg, T.S. Pedersen, F.B. Bendixen, N. Mijatovic, B.B. Jensen, and J. Holboll, in *2016 22nd International Conference on Electrical Machines, ICEM 2016* (Institute of Electrical and Electronics Engineers Inc., 2016), pp. 1625–1629.
116. C. Handwerker and B. Olson, Value Recovery Project, Phase 2. (2019). [http://thor.inemi.org/webdownload/2019/iNEMI-Value\\_Recovery2\\_Report.pdf](http://thor.inemi.org/webdownload/2019/iNEMI-Value_Recovery2_Report.pdf).
117. P. Upadhyay, M. Awais, A.K. Lebouc, L. Garbuio, M. Degri, A. Walton, J.C. Mipo, and J.M. Dubus, in *7th International IEEE Conference on Renewable Energy Research and Applications, ICRERA 2018 (Institute of Electrical and Electronics Engineers Inc., 2018)*, pp. 846–852.
118. K. Binnemans, P.T. Jones, B. Blanpain, T. van Gerven, Y. Yang, A. Walton, and M. Buchert, *J. Clean. Prod.* 51, 1 (2013).
119. K. Baba, E. Yuzo, and H.T. Nemoto, *Hitachi Rev.* 62, 452 (2013).
120. L. Cong, H. Jin, P. Fitsos, T. McLntyre, Y. Yih, F. Zhao, and J.W. Sutherland, *Procedia CIRP* 29, 680–685 (2015).
121. T.R. Simon, L. Cong, Y. Zhai, Y. Zhu, and F. Zhao, *Procedia CIRP* 69, 916–920 (2018).
122. T. Klier, F. Risch, and J. Franke, in *2013 IEEE International Symposium on Assembly and Manufacturing, ISAM 2013* (2013), pp. 88–90.
123. S. Hogberg, J. Holboll, N. Mijatovic, B.B. Jensen, and F.B. Bendixen, *IEEE Trans. Magn.* 53, 1 (2017).
124. Z. Li, A. Kedous-Lebouc, J.M. Dubus, L. Garbuio, S. Personnaz, and E.P.J. Appl. Phys. 86, 20901 (2019).
125. M. Orefice, A. Eldosouky, I. Škulj, and K. Binnemans, *RSC Adv.* 9, 14910 (2019).
126. M. Aoki and S. Hashimoto, US7143507B2 (31 March 2006).
127. A. Walton, H. Yi, N.A. Rowson, J.D. Speight, V.S.J. Mann, R.S. Sheridan, A. Bradshaw, I.R. Harris, and A.J. Williams, *J. Clean. Prod.* 104, 236 (2015).
128. M. Zakotnik, I.R. Harris, and A.J. Williams, *J. Alloys Compd.* 469, 314 (2009).
129. T. Kawasaki, M. Itoh, and K.I. Machida, *Mater. Trans.* 44, 1682 (2003).
130. C. Li, W.Q. Liu, M. Yue, Y.Q. Liu, D.T. Zhang, and T.Y. Zuo, *IEEE Trans. Magn.* 50, 1 (2014).
131. W. Liu, C. Li, M. Zakotnik, M. Yue, D. Zhang, and X. Huang, *J. Rare Earths* 33, 846 (2015).
132. X. Li, M. Yue, M. Zakotnik, W. Liu, D. Zhang, and T. Zuo, *J. Rare Earths* 33, 736 (2015).
133. D. Dupont and K. Binnemans, *Green Chem.* 17, 2150 (2015).
134. T. Vander Hoogerstraete and K. Binnemans, *Green Chem.* 16, 1594 (2014).
135. D. Prodius, K. Gandha, A.V. Mudring, and I.C. Nlebedim, *ACS Sustain. Chem. Eng.* 8, 1455 (2020).

**Publisher's Note** Springer Nature remains neutral with regard to jurisdictional claims in published maps and institutional affiliations.